Long Passage Times of Short ssDNA Molecules through Metallized Nanopores Fabricated by Controlled Breakdown

Harold Kwok, Matthew Waugh, José Bustamante, Kyle Briggs, and Vincent Tabard-Cossa**

The fabrication of individual nanopores in metallized dielectric membranes using controlled breakdown directly in solution is described. Nanopores as small as 1.5-nm in diameter are fabricated in Au-coated silicon nitride membranes immersed in 1 M KCl by subjecting them to high electric fields. The physical and electrical characteristics of nanopores produced with this method are presented. The translocation of short single-stranded DNA molecules is demonstrated through such nanopore devices without further passivation of the metallic surface. Metallized nanopores can prolong the translocation times of 50-nt ssDNA fragments by as much as two orders of magnitude, while the slowest events can reach an average speed as slow as 2 nucleotides per millisecond. The mechanism for the long dwell-time distribution is differentiated from prior studies, which relied on friction to slow down DNA, and is attributed to nucleotide-Au interactions.

1. Introduction

Solid-state nanopores are the subject of intense research efforts aimed at the development of disruptive, single-molecule sensing technologies with applications in DNA and protein sequencing.[1–3] Although electronic sequencing has been shown to be feasible using biological nanopores,[4–6] the robustness, flexibility in size and shape, and compatibility with wafer-scale technologies of solid-state nanopores still make them highly attractive, especially for the prospect of low-cost, scalable manufacturing of nanopore-based devices, and to diversify the breadth of applications. Yet, some challenges remain for solid-state nanopores to reach their full potential.

Sequence specific information obtained from ionic conductance measurements through a simple solid-state nanopore in an insulating membrane is generally limited.[7] The signal is bounded by physical constraints like instrumentation bandwidth, intrinsic electrical noise, spatial resolution, and thermal fluctuations.[8–10] For this reason, some groups have explored advanced functionalization of nanopore devices by designing more complex structures. These structures include multilayered membranes,[11,12] metallized dielectric membranes with or without molecular coatings,[13–15] and membranes equipped with nanoelectrodes.[16–20] In all these cases, the architecture of these advanced nanopore devices involve at least one conductive metallic film. Such conductive layers are intended to read alternative electrical signals, such as an induced charge,[21,22] potential[23] and transverse tunneling current,[24] or to control the motion of biopolymers during passage by modulating a local electric field,[25] or by providing binding sites for biomolecules.[14] However, the throughput at which these complex structures can be tested under different operating conditions is a major bottleneck that impedes faster progress in the field. This is, in part, a consequence of the nanopore fabrication approaches currently being employed, which negatively affects the yield of functional devices. Nanofabrication strategies relying on beams of energetic particles, either electrons or ions, require expensive, complex equipment that are inherently low throughput and involve multiple handling steps. Recently, our group has demonstrated that dielectric breakdown can be utilized to create individual nanopores on bare insulating solid-state membranes[26] and reliably achieve sub-2-nm feature size.[27] In addition, this technique creates nanopores directly in an aqueous solution, thus completely eliminating issues related to wetting and significantly reducing handling risks. The simplicity in fabrication and workflow offered by the method will likely help increase the research output of many groups and render the field accessible to others. Nevertheless, the capacity of this method to fabricate nanopores in more complex membrane structures remains to be explored. This article describes the fabrication of individual nanopores on metallized dielectric membranes using controlled breakdown (CBD), and introduces a high-electric field pulsing strategy where the voltage across the metallized membrane is stepped between a long, low monitoring voltage and a brief, higher fabrication voltage. Finally, the translocation kinetics of short single-stranded DNA molecules through these metallized nanopores is presented. This study lays the foundation for future work to employ CBD for the fabrication of nanopores in more complex membrane structures, incorporating metallic materials, such as nanofluidic transistors or devices equipped with nanoelectrodes.

H. Kwok, M. Waugh, J. Bustamante, K. Briggs, Prof. V. Tabard-Cossa
Department of Physics, University of Ottawa
150 Louis Pasteur
Ottawa, Ontario K1N 6N5, Canada
E-mail: harold.kwok@uOttawa.ca
E-mail: tcossa@uOttawa.ca

DOI: 10.1002/adfm.201402468

2. Results and Discussion

In previous work, we reported the fabrication of individual solid-state nanopores on bare SiN_x and SiO_2 membranes via controlled dielectric breakdown in solution.[26] The method allows for rapid and low-cost fabrication of nanopores for single-molecule detection simply by generating high electric fields inside dielectric membranes using standard Ag/AgCl electrodes. This article extends a similar experimental protocol to fabricate individual nanopores on metallized dielectric membranes. In this work, we use 10-nm thick SiN_x membranes coated with 30-nm metal films (5-nm of Cr, 25-nm of Au) as described in the Methods section. To fabricate a nanopore, we mount the metallized membrane in a liquid cell so as to separate two reservoirs, which are filled with filtered and degassed 1 M KCl, buffered at pH 10. To initiate the nanofabrication process, a leakage current across the metallized dielectric membrane is induced by applying a voltage across the two reservoirs in the range of 3–18 V. A custom resistive feedback current amplifier circuit connected to a computer is set to monitor the leakage current at 100-Hz. We have tested two different voltage schemes to expose the metallized membrane to high electric fields. The first approach follows Kwok et al.[26], where a constant voltage is applied until a breakdown event occurs, at which point the leakage current abruptly increases and crosses a given threshold value, triggering the termination of the applied voltage. The second approach relies on the application of a square voltage pulse between a low monitoring voltage and a high fabrication voltage. The monitoring voltage, set at 200 mV, is used to detect the presence of ionic current from a newly formed nanopore. A current trace of each scheme is illustrated in **Figure 1**. In Figure 1b, the fabrication and monitoring pulse have a width of 50-ms and 1-s respectively. We found that both schemes can reliably fabricate a nanopore at either voltage polarity, and in conditions similar to fabrication on bare dielectric membranes. The pulsing approach eliminates the need to set an arbitrary leakage current threshold, which is experiment dependent, at the expense of a higher variance in fabrication time and overall longer fabrication process (see Supporting Information Section S1 for a list of tested fabrication conditions).

The physical conditions of nanopores and of the metallized membranes surfaces following fabrication by CBD were examined by optical microscopy and transmission electron microscopy (TEM). Optical examination of the metallized chip under a stereomicroscope equipped with episcopic illumination revealed no observable physical changes to the Au film. The metallic layer remains intact and laminated. Under TEM, a 30-nm thick metallized layer is far less transmissive than bare SiN_x or vacuum, thus enabling high contrast imaging against a nanopore formed in the layered membrane, and somewhat facilitating the localization of a nanopore within the 50 μm × 50 μm membrane area. However, locating a sub-10-nm nanopore in a 2500-μm^2 area remains challenging. **Figure 2** shows two nanopores, created on two different Au-coated SiN_x membranes. The images show that a hole is formed through both the metal and the dielectric layer. From the TEM images, the

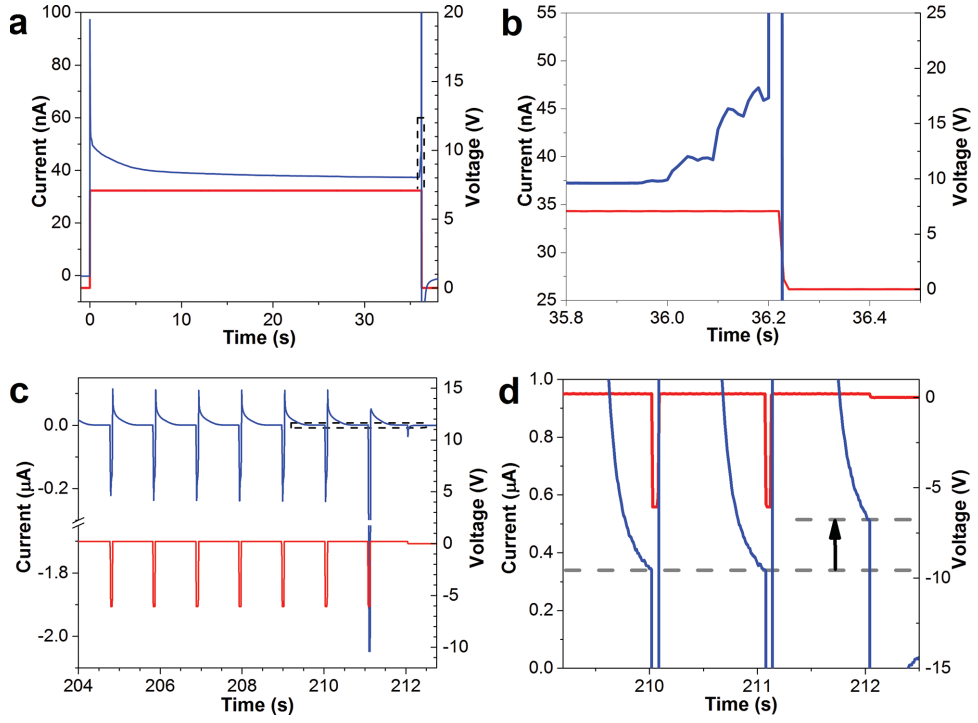

Figure 1. Current (blue) and voltage (red) traces during the fabrication of two metallized nanopores illustrate that breakdown can occur at both polarities and for both fabrication approaches. The regions marked by a dash-rectangle in (a,c) are enlarged in (b,d) respectively. a) Fabrication with a constant applied voltage of +7 V. c) Fabrication with a repeating 50-ms pulse at –6 V. A monitoring period of 1 s, biased at +200 mV is inserted between each fabrication pulses. Spikes in both directions are caused by capacitive current, in response to a sudden change in voltage. d) The black arrow indicates the increase in current in the monitoring period, attributed to the appearance of ionic current from a newly fabricated nanopore (formed at ≈211 s). The voltage bias is set to zero as soon as ionic current is detected.

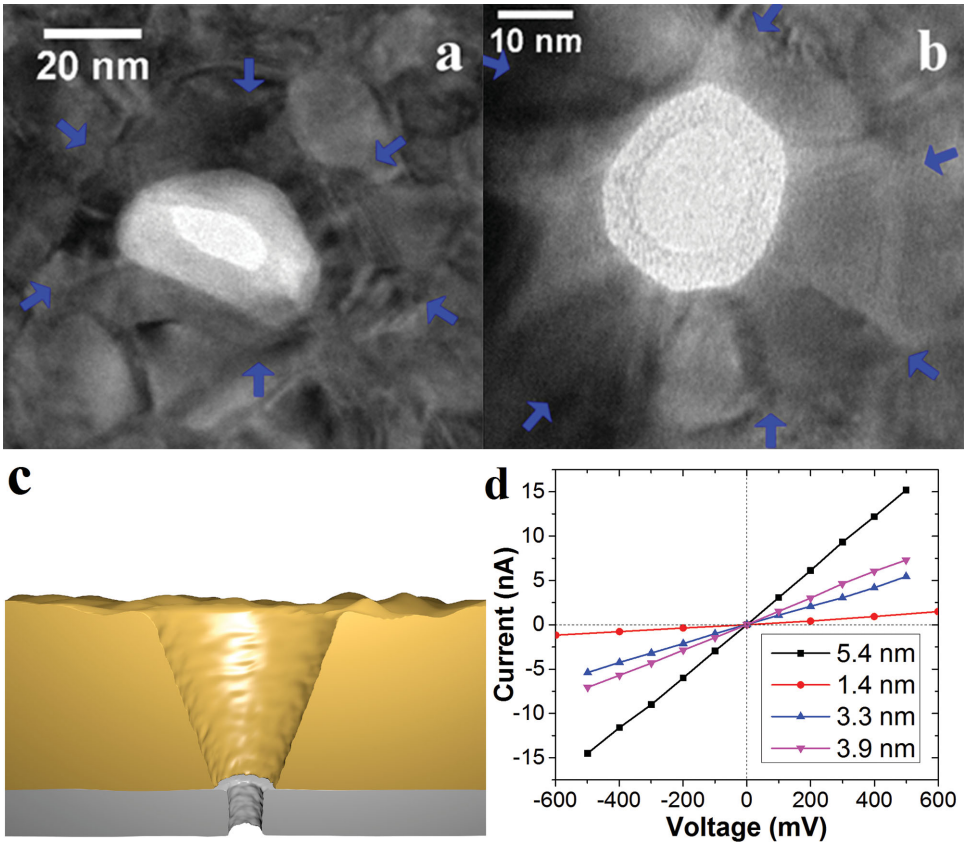

Figure 2. a,b) Bright field TEM images of two metallized nanopores, each with a different SiN_x membrane thickness, giving rise to a different contrast against a nanopore. Gold recedes away from, and is concentric to, the nanopore rim. Arrows outline the top opening of the metal channel. The effective diameter, *d*, and length, *l*, of the nanopores are in a) $d = 13$ nm, $l = 30$ nm, and in b) $d = 15$ nm, $l = 10$ nm. c) Cross-sectional view of an illustration of the geometry of a metallized nanopore, infered from TEM data. $d = 5.4$ nm $l = 10$ nm. d) *I–V* curves of 4 different metallized nanopores on 10-nm thick SiN_x membranes.

opening through the Au layer appears to be larger than the hole in the silicon nitride, thus exposing some bare SiN_x around the rim of the nanopore. Furthermore, while the nanopore through the SiN_x layer has a cylindrical or elliptical shape, the opening through the metal layer appears to be conical, closing in size towards the nanopore. In Figure 2a,b, the top opening on the metal surface is outlined by arrows. A schematic representation of the nanopore fabricated by CBD is shown in Figure 2c. The concentric and conical shape of the metallic opening may suggest that electrochemical etching, along the electric field lines extending away from the nanopore, is involved in the removal of Au and Cr as the nanopore was formed, in contrast to physical rupturing; although the precise mechanism for material removal is unknown at this time.

Nanopores are electrically characterized immediately after fabrication by measuring their ionic current behavior in 1 M KCl pH10 and 3.6 M LiCl pH8. Figure 2d shows *I–V* curves of 4 fabricated nanopores. On some occasions, we have observed the rapid enlargement of metallized nanopores under voltage bias greater than 500 mV. Although a nanopore can be enlarged by high electric fields,[28] we have found that metallized nanopores are generally more susceptible to field-driven enlargement than bare silicon nitride nanopores. Considering that the metal is left floating in all of our experiments, when the bias of the solution in contact with the Au layer is above the interface overpotential, the metal should be at equipotential with the electrolyte. The voltage drop is thus not only concentrated inside the nanopore in the SiN_x membrane but also at the Au/SiN_x interface, which we believe leads to enlargement under lower applied voltages. However, within a ±500 mV voltage range, these metallized nanopores exhibit Ohmic *I–V* responses. The conductance extracted from these measurements can therefore be used to obtain physical dimensions for the nanopores. Assuming that the nanopore formed in the SiN_x layer has a cylindrical geometry, and that the metal layer is at equipotential with the electrolyte, then the length of a pore, *l*, is equal to the thickness of the SiN_x membrane and the thickness of the metal can be ignored. Hence the effective diameter, *d*, of a cylindrical nanopore is related to the conductance, *G* by:[14,29]

$$G(d) = \sigma\left[\frac{4l}{\pi d^2} + \frac{\alpha}{d}\right]^{-1} \quad (1)$$

In this equation, σ is the conductivity of the electrolyte inside the nanopore. The second term denotes the access resistance. When a pore is symmetrical with an access resistance on both side of the pore opening, then $\alpha = 1$, while when access

Table 1. Nanopore diameters calculated from open pore conductance (Equation 1) and DNA blockage model (Equation 2). Effective diameters are evaluated at both $\alpha = 0.5$ and $\alpha = 1$ as listed.

	Ionic Conductance Model (Equation 1)			DNA Blockage Model (Equation 2)	
$V_{applied}$	$I_{open\ pore}$	σ	$d\{\alpha = [0.5/1]\}$	$\Delta I/I$	$d\{\alpha = [0.5/1]\}$
–200 mV	6.1 ± 0.5 nA	16.08 S/m	[5.4/6.0] ± 0.2 nm	0.062 ± 0.008	[5.4/5.2] ± 0.3 nm
–300 mV	9.3 ± 0.8 nA	16.08 S/m	[5.5/6.0] ± 0.3 nm	0.062 ± 0.015	[5.4/5.2] ± 0.7 nm

resistance on one side is suppressed by a metallic material, then $\alpha = 0.5$. Considering that ssDNA molecules can be captured from the metallized side, and that the applied voltage influences the capture rate, the electric field must also extend outside of the nanopore on the metallized side. Thus, α in the access resistance term can be taken to vary between 0.5 and 1. Diameters of nanopores calculated from conductance measurements using Equation 1 are compared with that obtained from DNA current blockages, and are presented in **Table 1**. Results suggest that the cylindrical assumption with $\alpha \cong 0.5$ is reasonable and provides a good measurement of the nanopore effective size, although the effect of α on the calculated nanopore size is relatively minor.

We performed DNA translocation experiments to verify the ability of the metallized nanopores fabricated by high electric fields to detect individual DNA molecules and explored their translocation kinetics. **Figure 3**a shows a set of ionic current traces taken at –200 mV and –300 mV for a 5.4 nm nanopore, as calculated from conductance measurements in 3.6 M LiCl (see Figure 2d) with $\alpha = 0.5$. Under this polarity, DNA molecules from the metal-coated side of the membrane are electrophoretically driven through the nanopore towards the SiN_x side of the membrane (see Methods section). The ionic current blockages during the passage of 50-nt ssDNA are qualitatively similar to electrical signals observed on bare SiN_x membranes using either TEM-drilled nanopores or pores fabricated by CBD.[26] DNA capture rate is found to be dependent on applied voltage and corresponds to ≈1.5 Hz for –200 mV and ≈10 Hz for –300 mV. Figure 3b–d shows individual translocation events at –300 mV for linear, partially folded, and fully folded ssDNA molecules respectively.

Ionic blockage current level of single-level events, ΔI, caused by translocations of DNA molecules in a linear configuration provides an alternative method to estimate a pore size. Assuming a DNA molecule spans the entire length of a SiN_x pore when it translocates through, the normalized ionic blockage current is given by:[29]

$$\frac{\Delta I}{I} = \frac{\Delta G}{G(d)} = 1 - G(d')/G(d) \quad (2)$$

where $d' = \sqrt{d^2 - d_{DNA}^2}$ is the effective cross-section diameter of a pore when a DNA molecule is present. A 50-nt ssDNA molecule, at the salt concentration used, has a persistence length of 1–2 nm[30] and a contour length of ≈30 nm. Since the contour length is longer than several persistence lengths, a molecule can translocate in a folded (two, or more, quantized current levels) or linear (unfolded, single-level events) conformation. The time-averaged ionic current blockage level of an event should then be bounded by the unfolded configuration and the highest-order possible folded configuration during passage. As shown in Figure 3, we predominantly observe single and double blockage levels, in agreement with the steric possibilities

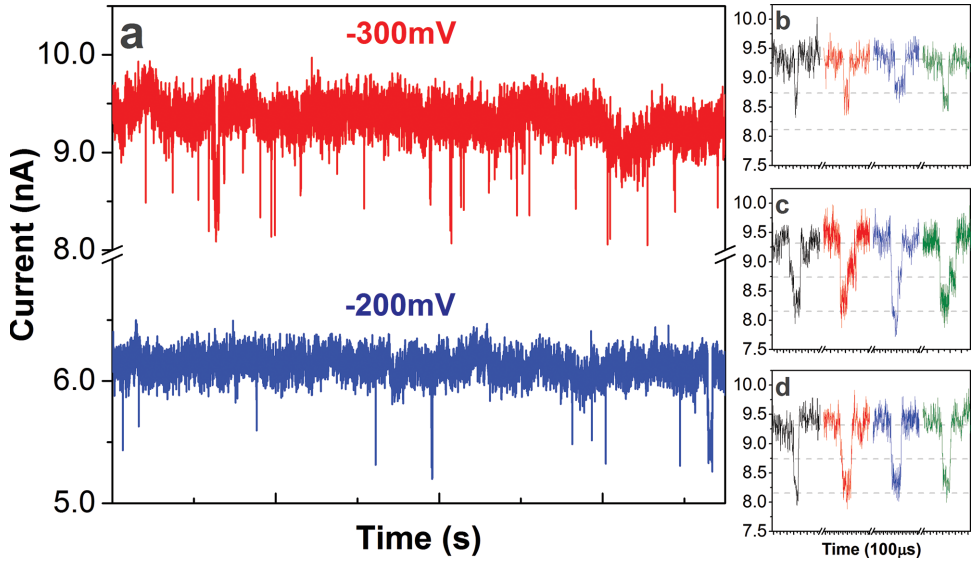

Figure 3. a) Ionic current traces of ssDNA translocations through the metallized pore driven at –200 mV and –300 mV. b–d) Individual translocation events at –300 mV. The dashed line indicates the baseline current (9.32 nA), the expected single blockage level (6.25%), and the double blockage level (12.5%) calculated with Equation 2. b) Unfolded translocations, c) partially folded translocations, d) fully folded translocations.

offered by the nanopore size. Substituting the experimental value of $\Delta I/I = 0.062$, for the average relative blockage level of linear conformation, into Equation 2 provides an alternative method to evaluate the effective pore diameter. Values are shown in Table 1. Using $d_{DNA} = 1.4$ nm yields an effective pore diameter of 5.4 nm, which agrees very well with the diameter acquired from conductance measurement with Equation 1, and supports the cylindrical geometry assumption using the nominal SiN_x membrane thickness as the nanopore length.

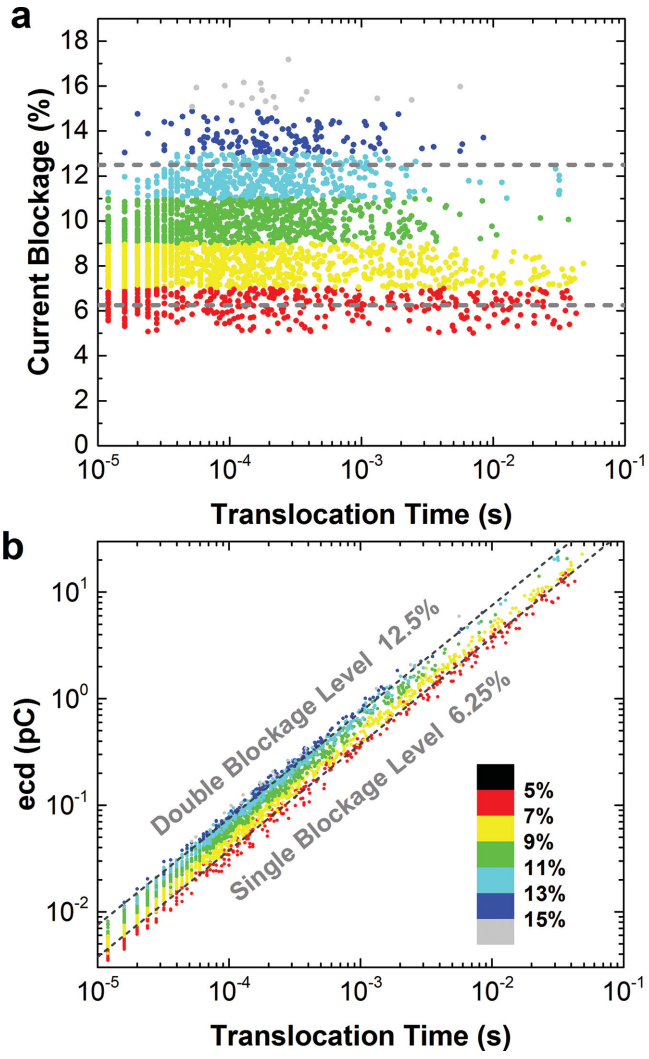

Figure 4. Data points are color-mapped to distinct current blockage levels, based on scale shown in (b) to assist in the comparison with the ecd data in (b). Data points on the left end are aligned vertically due to our particular choice of sampling rate, which limits time resolution to 4-μs intervals. a) Scatter plot of the normalized average current blockade versus the total translocation time for 50-nt ssDNA molecules at –200 mV. The relative blockage level is defined with respect to the open pore current (0% representing a fully opened pore, and 100% a fully blocked pore). Translocation time is plotted in log scale. The two dashed lines represent the expected single and double blockage levels, 6.25% and 12.5% respectively, calculated with Equation 2. b) Log–log plot of ecd versus translocation time. The ecd of an event is the product of the translocation time and the time-averaged blockage current.

Figure 4a shows a scatter plot of the percent current blockage as a function of passage time for all translocation events obtained at –200 mV. Single level events, characteristic of the passage of linearized molecules, exhibit an average current blockage of 6.2% relative to the open pore current. Notably, translocation times for the passage of short 50-nt ssDNA molecules span multiple orders of magnitude, ranging from a few microseconds to tens of milliseconds. This clearly indicates that the event charge deficit (ecd), that is, the measured time integral of blocked ionic current, is not conserved, which is contrary to what is expected for electrophoretically driven passage in pores of this size.[31] This is further revealed when ecd is plotted as a function of translocation time as shown in Figure 4b, showing a non-zero slope. The non-conserved ecd implies that the average translocation speed varies greatly amongst strands of identical length, and suggests the presence of strong interactions between the DNA and the walls of the nanopore.

The long dwell-time passage of short ssDNA shown in Figure 4a could potentially originate from two or more ssDNA fragments entering a pore simultaneously, though mutual repulsion should minimize such an occurrence. To verify that registered events are indeed full translocations of individual ssDNA molecules, ecd is plotted against the translocation time in log-log scale in Figure 4b. Multiple DNA molecules entering the pore simultaneously would cause higher current blockage levels than single-level events. If long lasting events were caused by multiple molecules entering the pore simultaneously, the data points in Figure 4b would increasingly deviate away from the single blockage level as translocation time increases. On the contrary, the data points fall closely within the single and double blockage levels, and exhibit a straight line in log–log scale with a slope (power) of 1. Of note from Figure 4a,b is the fact that for very long translocation times (>3 ms) single-level events are favored. This observation implies that the slowing down mechanism at play here is distinct from friction dominated kinetics previously observed on bare SiN_x pores,[32] as one would expect folded ssDNA to cause increased friction with the nanopore wall.[33]

To highlight the slowed ssDNA translocation kinetics through metallized nanopores, we compare these results with data obtained on a bare SiN_x nanopore of similar size. Identical ssDNA translocation experiments were performed on the two separate nanopores at –200 mV and –300 mV. The observed ionic current blockade levels produced by the translocation of 50-nt ssDNA molecules on a bare SiN_x nanopore compare very well with the data on a metallized nanopore (see Table 1). This further supports our assumption that most of the potential drop is across the insulating silicon nitride portion of the membrane for metallized nanopores fabricated by CBD. The two nanopores must therefore have similar effective diameters and lengths. The normalized histograms of log-translocation time are shown in semi-log scale in **Figure 5**. It is clear that metallized nanopores significantly extend the translocation time, by as much as two orders of magnitude, with the median prolonged by roughly one order of magnitude. The upper bound of translocation times corresponds to an average speed of 2-ms per nucleotide, although we do not expect nucleotides in a strand to necessarily translocate at a uniform speed. It is

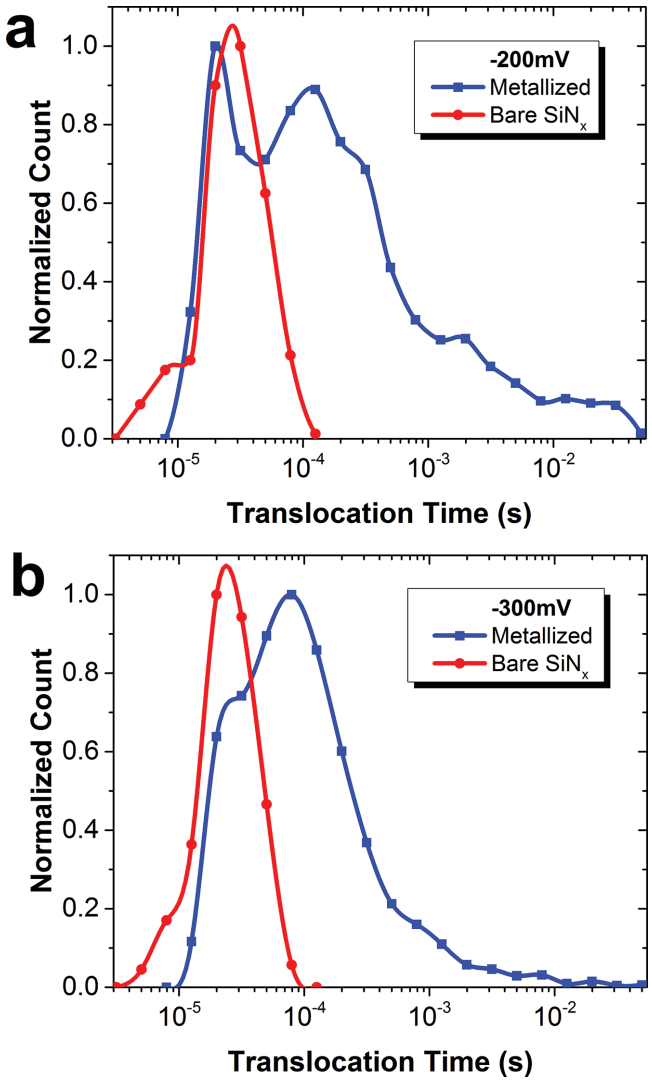

Figure 5. Histogram of log-translocation-time taken at: a) –200 mV (2,787 events) and b) –300 mV (5254 events). Counts of each set are normalized to their maximum value for the purpose of comparison. Translocation experiments are carried out on a bare SiN_x nanopore (d = 5.2 nm, l = 10 nm) and the metallized nanopore (d = 5.4 nm, l = 10 nm). Solid spline lines are used to connect the data points within a set.

more likely that given the strong adenine-Au interactions,[34–36] a single-stranded polyadenine DNA molecule would be temporarily interrupted by the Au surface as it translocates due to their binding affinity (i.e., stick-slip type motion). Besides the extended translocation times, the distribution is also highly heavy-tailed, characterized by a non-linear decay when plotted in log scale, implying that the observed long lasting translocations events are not rare. Furthermore, a comparison between the –200 mV and –300 mV data sets reveals that the tail of the distribution towards long passage times is voltage dependent, in agreement with a force-dependent distribution of dissociation times of nucleotide-Au bonds.

Further investigation of the histogram data between metallized and bare SiN_x nanopores indicates that there are two distinguishable peaks in a distribution for the metallized nanopore data. Considering the fact that the peaks at the lower bound from both sets of data overlap closely, we argue that this sub-population of translocation events originates from translocations in the absence of, or with very weak, Au-DNA interactions. Based on the metallic nanopore geometry extracted from TEM images (Figure 2), which indicates that the Au layer is slightly receded from the edge of the nanopore formed in the SiN_x layer, it is possible for a DNA molecule to be captured by the pore and to translocate close to the central axis, without coming into contact with the metal surface.

To support the interpretation of ssDNA-Au interactions as a mechanism for slowing down translocations, two additional control experiments were performed and are shown in **Figure 6**. The first experiment involves the translocation of 50-nt ssDNA fragments in the reverse direction (from SiN_x to metallic side) using a metallized nanopore with d = 4.9 nm. In this direction, DNA strands will not encounter the Au layer until they exit the SiN_x portion of the nanopore (i.e., the detection region), and the kinetics of translocation should, in principle, not be affected by the presence of the metal surface. Through this experiment, interactions between ssDNA, the SiN_x pore wall and the metallic layer can be distinguished. A scatter plot of the normalized average current blockade versus the total passage time, and a histogram of the passage times are shown in Figure 6a,c respectively. The vast majority of the events translocate the metallized nanopore in this direction under 100 µs. This suggests that ssDNA molecules have only weak interactions with the pore wall. Furthermore, in contrast to data shown in Figure 5, the distribution of passage times in this reverse direction does not exhibit two peaks or a significant broadening. The histogram decays rapidly (i.e., long-lived events are rare) as shown in Figure 6c. This data set supports our interpretation that the prolonged events seen in the forward direction (from Au to SiN_x side) are due to ssDNA-Au interactions during passage. A separate control experiment, involved the translocation of 50-bp double-stranded DNA (dsDNA) through a d = 5.8 nm metallized nanopore. In this case, hydrogen bonding with the Au surface is restricted since only the phosphate backbone of the nucleic acid molecule is exposed. A much weaker dsDNA-Au interaction is therefore expected, especially since the Au layer is in the negatively biased reservoir. Results are shown in Figure 6b,d. The histogram in Figure 6d reveals a single narrow peak, with a most probable passage time below 10 µs, indicating no noticeable increase in translocation times. The low capture rate that was observed also suggests that the bulk of the events are too fast to be detected, in-line with what is expected for the translocation of short dsDNA molecules through bare SiN_x nanopores, 5–6 nm in size.

The experimental data presented in this article point to the fact that the Au layer is interacting strongly with the ssDNA and is likely the cause of the exceptionally long dwell times. This is consistent with prior knowledge that ssDNA can be physisorbed to gold surfaces in a base specific way.[34–36] In particular, adenine interacts with gold most strongly. Accordingly, we can present the following picture, in line with the observations. **Figure 7** illustrates the two possible scenarios in which a ssDNA molecule is electrophoretically driven from the metal side to SiN_x side. Recall that from the analysis of the

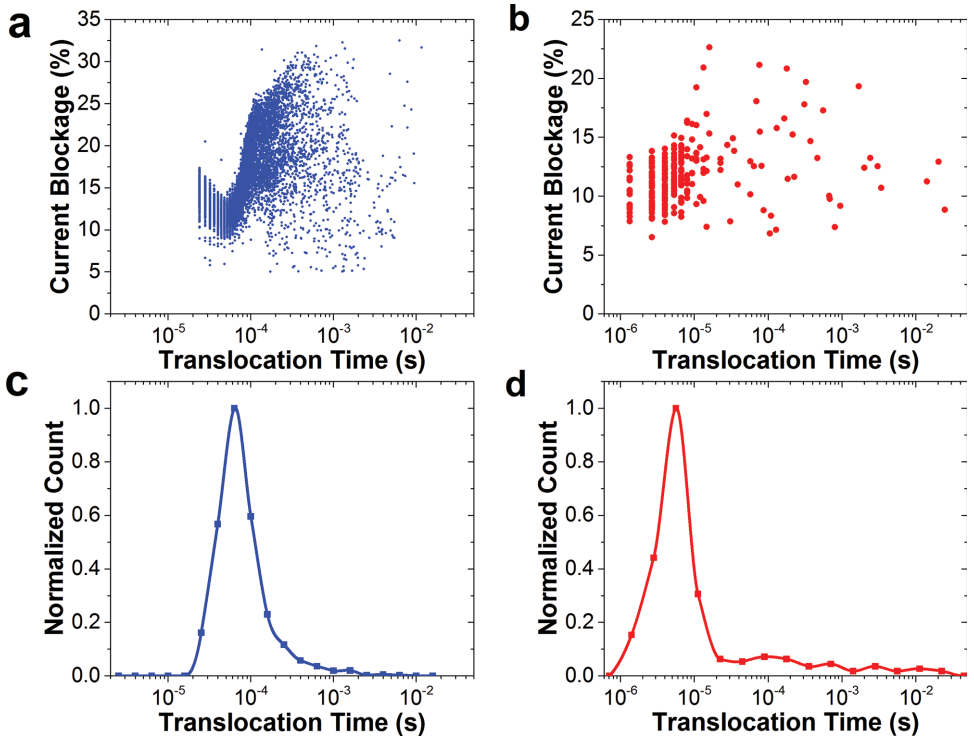

Figure 6. a) Scatter plot of the normalized average current blockade versus the total translocation time of a single-molecule event. Each of the 14 461 points represents a single ssDNA translocation event. 50-nt ssDNA fragments are captured from the SiN_x side of the metallized pore ($d = 4.9$ nm, $l = 10$ nm) by an applied voltage of +200 mV (i.e., reversed direction). We attribute the slightly longer translocation times of deeper blockages to increased friction between folded ssDNA molecules and the pore wall. b) Scatter plot of 398 events of 50-bp dsDNA fragments translocating through a metallized pore ($d = 5.8$ nm, $l = 10$ nm), from the metallic side at –300 mV (i.e., forward direction). Figure (c,d) are normalized histograms of translocation times of a) and b) respectively. A segment of the corresponding current traces are given in Supporting Information S4.

translocation data, we expect that most of the potential drop, and hence the electrophoretic driving force, to be across the insulating SiN_x portion of the membrane. In Figure 7a, both ends of the ssDNA are physisorbed onto the gold surface leading to a folded entry of the molecule into the SiN_x portion of the nanopore, thus producing long-lived double-level events. In Figure 7b, during capture most of the ssDNA fragment is physisorbed onto the gold surface, leaving only one short end of the ssDNA to enter the pore, leading to single-file passage. These single-level events can be longer-lived than folded translocations if they initially experience less electrophoretic pulling force due to a smaller number of nucleotides inside the pore, while also experiencing stronger pinning from the longer proportion of their chain being physisorbed to the gold. This would explain why data points of long dwell times are inclined toward the single blockage level.

3. Conclusion

In summary, we demonstrated that controlled breakdown can be utilized to fabricate more complex nanopore structures comprising both metallic and dielectric materials. We showed that metallized nanopores produced using this method are compatible with single molecule sensing of DNA molecules. The metal layer in the vicinity of the opening of the nanopore interacts strongly with single-stranded DNA, resulting in exceptionally long passage times for these short molecules, in contrast to double-stranded DNA molecules of similar size. The observed translocation kinetics are believed to be sensitive to the initial molecular conformation and the length of DNA interacting with the metallic surface. Nevertheless, such metallized nanopores could be used to selectively slow down the translocation kinetics of short dsDNA fragments tagged at their ends with short ssDNA extensions for a type of biomarker detection assay. More generally, however, we anticipate this work will provide a new strategy to fabricate a nanopore equipped with nanoelectrodes for actuation or sequencing applications by single-molecule tunnelling spectroscopy.

4. Experimental Section

Metal Deposition on Membrane: In this study, we employed commercially available free-standing silicon nitride membranes 50-μm × 50-μm in size located at the center of a 3 mm in diameter, 200-μm thick silicon support chip, as the starting point of our fabrication process (TEM windows from Norcada NT005Z and NT005X). These TEM windows have a 10-nm or 30-nm thick non-stoichiometric silicon nitride (SiN_x) layer, deposited by low-pressure chemical vapor deposition (LPCVD). The resulting silicon nitride is amorphous, slightly silicon rich and low in tensile stress. Prior to metal deposition via e-beam evaporation, the SiN_x membranes are plasma cleaned at 30 W for 60 s. A 5-nm Cr adhesive layer is first deposited, followed by 25 nm of Au. The metallic layer is deposited onto a circular area of ca. 1-mm in diameter at the center of the chip, defined by an Al shadow mask. This prevents metals from being deposited on the edge of

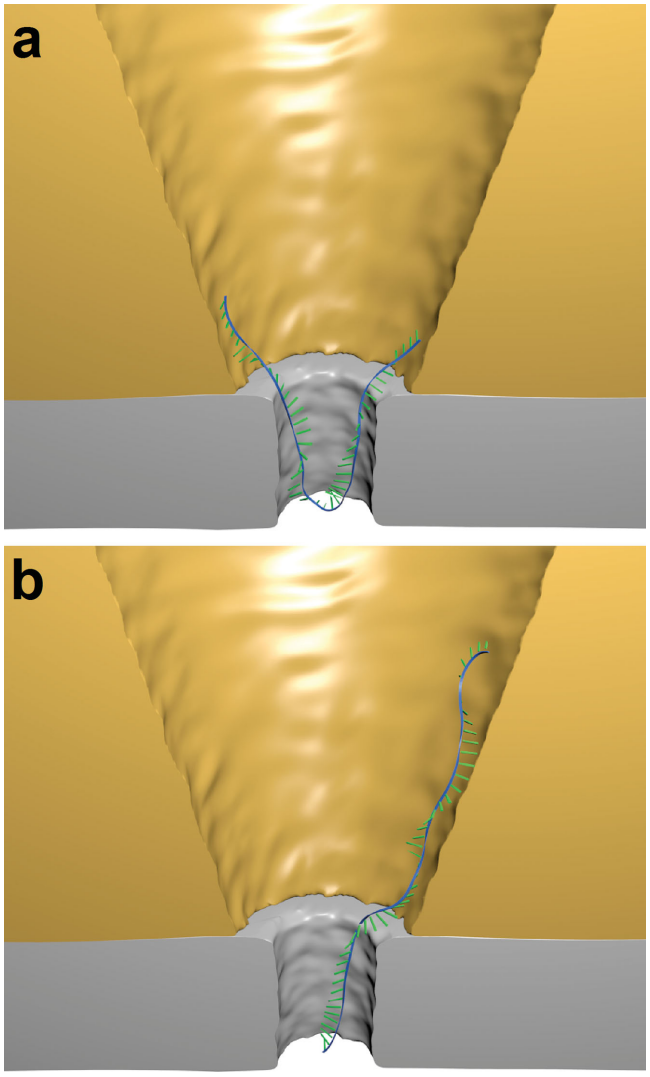

Figure 7. Illustration of translocation dynamics of a 50-nt ssDNA through a metallic nanopore. The ssDNA has a contour length of 33 nm. The SiN_x nanopore has dimensions: $d = 6$ nm, $l = 10$ nm. a) Small segments of both ends of the ssDNA molecule are being adsorbed on the metallic surface. b) A single large segment of the ssDNA molecule is adsorbed on the metallic surface.

a chip, where the insulating SiN_x is often damaged, exposing the doped silicon substrate, which could create an alternative electrical pathway for the leakage current across the two sides of the chip.

Mounting and Wetting Procedures: The metallized membrane is placed in a custom designed polyether ether ketone (PEEK) cell as to separate two 200-µL fluidic reservoirs, each containing an Ag/AgCl electrode. Custom silicone elastomer gaskets are used to form a liquid tight seal between the two sides of the membrane. To ensure proper wetting of the membrane, each reservoir is first filled with 95% ethanol before switching to water and finally the aqueous salt solution used for fabrication. All solutions used were filtered and thoroughly degassed. Since the wet state of the membrane cannot be directly verified by resistance measurement, we instead evaluate the capacitance of the immersed chip with a digital multimeter (Agilent 34405A). For our experimental setup, when the membrane is fully wetted, a capacitance value >200 pF is measured in 1 M KCl.

DNA Translocation Measurements and Analysis: For ssDNA experiments, ionic current through a nanopore is monitored by a commercial patch-clamp amplifier (Axopatch 200B), with a 4-pole Bessel filter set at 100 kHz. Current traces are digitized at 250 kHz by a DAQ card (National Instruments, PXI-6361) and then recorded in a computer using custom LabView software. Short single-stranded DNA (ssDNA), 50-nt in length, with sequence $(dA_9dC)_5$, synthesized by Integrated DNA Technologies Inc, are used in this study. For dsDNA (Thermo Scientific NoLimits DNA fragments 50-bp) translocation experiments, a Multiclamp 700B is used, with analog filter bypassed and sampling set at 750 kHz. All DNA translocations are performed in 3.6 M LiCl, 10 mM HEPES pH8. Li^+ is used to promote slower translocation times due to the stronger screening of the DNA charge compared to K^+.[37] In all experiments, 100-pmole of ssDNA was mixed thoroughly with 200-µL of electrolyte at the cathode reservoir, yielding a molar concentration of 0.5-nM. Throughout this work, the reference point (ground) for all voltages quoted is the silicon nitride side of the membrane (i.e., opposite to the metallic side). Translocation events, registered as discrete drops in current, are detected and analyzed by custom LabView software. The relatively large area of metal exposed to the electrolyte gives rise to significant high-frequency noise, due to the increased chip capacitance compared to uncoated membranes.[8,13] If an experiment required, this extra noise could be removed by patterning of the metal layer[13] or by painting PDMS[8] to reduce the surface area of the metal exposed to the electrolyte. In addition, ssDNA strands can be physisorbed onto the Au surface near the nanopore entrance, which can cause low-frequency current fluctuations (see Supporting Information Section S2 for noise characterization of our devices). In our experimental configuration, a ≈5.4-nm pore detecting ssDNA fragments has a signal-to-noise ratio of ≈2. This ratio improves to 3 when the data is digitally low-pass filtered at 20 kHz. However, even at this ratio, errors can occur while evaluating the translocation time of an event. Due to the large number of events detected, the error rate is estimated by sampling a random subset of data points at different orders of magnitudes in translocation time (see Supporting Information Section S3).

Supporting Information

Supporting Information is available from the Wiley Online Library or from the author. It contains tables summarizing nanopore fabrication conditions tested and error estimates on timing of translocation events, and figures showing the power spectrum density of ionic current through a metallized nanopore, and ionic current traces of control experiments.

Acknowledgments

This work was supported by the Natural Sciences and Engineering Research Council of Canada (NSERC), and the Canada Foundation for Innovation. J. Bustamante, K. Briggs and M. Waugh acknowledge the financial support provided by SENESCYT, NSERC, and OGS respectively, for Postgraduate Fellowships. The authors would like to thank Y. Liu for valuable technical support during TEM imaging.

Received: July 23, 2014
Revised: September 13, 2014
Published online: October 13, 2014

[1] J. Nivala, D. B. Marks, M. Akeson, *Nat. Biotechnol.* **2013**, *31*, 247.
[2] Y. Zhao, B. Ashcroft, P. Zhang, H. Liu, S. Sen, W. Song, J. Im, B. Gyarfas, S. Manna, S. Biswas, C. Borges, S. Lindsay, *Nat. Nanotechnol.* **2014**, *9*, 466.
[3] D. Branton, D. W. Deamer, A. Marziali, H. Bayley, S. a Benner, T. Butler, M. Di Ventra, S. Garaj, A. Hibbs, X. Huang, S. B. Jovanovich, P. S. Krstic, S. Lindsay, X. S. Ling, C. H. Mastrangelo, A. Meller, J. S. Oliver, Y. V Pershin, J. M. Ramsey,

R. Riehn, G. V Soni, V. Tabard-Cossa, M. Wanunu, M. Wiggin, J. a Schloss, *Nat. Biotechnol.* **2008**, *26*, 1146.
[4] J. Clarke, H.-C. Wu, L. Jayasinghe, A. Patel, S. Reid, H. Bayley, *Nat. Nanotechnol.* **2009**, *4*, 265.
[5] G. M. Cherf, K. R. Lieberman, H. Rashid, C. E. Lam, K. Karplus, M. Akeson, *Nat. Biotechnol.* **2012**, *30*, 344.
[6] E. A. Manrao, I. M. Derrington, A. H. Laszlo, K. W. Langford, M. K. Hopper, N. Gillgren, M. Pavlenok, M. Niederweis, J. H. Gundlach, *Nat. Biotechnol.* **2012**, *30*, 349.
[7] K. Venta, G. Shemer, M. Puster, J. A. Rodríguez-Manzo, A. Balan, J. K. Rosenstein, K. Shepard, M. Drndić, *ACS Nano* **2013**, *7*, 4629.
[8] V. Tabard-Cossa, D. Trivedi, M. Wiggin, N. N. Jetha, A. Marziali, *Nanotechnology* **2007**, *18*, 305505.
[9] J. D. Uram, K. Ke, M. Mayer, *ACS Nano* **2008**, *2*, 857.
[10] M. Zwolak, M. Di Ventra, *Rev. Mod. Phys.* **2008**, *80*, 141.
[11] B. M. Venkatesan, D. Estrada, S. Banerjee, X. Jin, V. E. Dorgan, M.-H. Bae, N. R. Aluru, E. Pop, R. Bashir, *ACS Nano* **2012**, *6*, 441.
[12] S. Harrer, P. S. Waggoner, B. Luan, A. Afzali-Ardakani, D. L. Goldfarb, H. Peng, G. Martyna, S. M. Rossnagel, G. A. Stolovitzky, *Nanotechnology* **2011**, *22*, 275304.
[13] R. Wei, D. Pedone, A. Zürner, M. Döblinger, U. Rant, *Small* **2010**, *6*, 1406.
[14] P. Krishnakumar, B. Gyarfas, W. Song, S. Sen, P. Zhang, P. Krstić, S. Lindsay, *ACS Nano* **2013**, *7*, 10319.
[15] R. Wei, V. Gatterdam, R. Wieneke, R. Tampé, U. Rant, *Nat. Nanotechnol.* **2012**, *7*, 257.
[16] E. S. Sadki, S. Garaj, D. Vlassarev, J. A. Golovchenko, D. Branton, *J. Vac. Sci. Technol. B Microelectron. Nanom. Struct.* **2011**, *29*, 053001.
[17] M. Puster, J. A. Rodríguez-Manzo, A. Balan, M. Drndić, *ACS Nano* **2013**, *7*, 11283.
[18] K. Healy, V. Ray, L. J. Willis, N. Peterman, J. Bartel, M. Drndić, *Electrophoresis* **2012**, *33*, 3488.
[19] A. P. Ivanov, E. Instuli, C. M. McGilvery, G. Baldwin, D. W. McComb, T. Albrecht, J. B. Edel, *Nano Lett.* **2011**, *11*, 279.
[20] A. P. Ivanov, K. J. Freedman, M. J. Kim, T. Albrecht, J. B. Edel, *ACS Nano* **2014**, *8*, 1940.
[21] Y. Liu, D. E. Huber, V. Tabard-Cossa, R. W. Dutton, *Appl. Phys. Lett.* **2010**, *97*, 143109.
[22] Y. Liu, J. Sauer, R. W. Dutton, *J. Appl. Phys.* **2008**, *103*, 084701.
[23] G. Sigalov, J. Comer, G. Timp, A. Aksimentiev, *Nano Lett.* **2008**, *8*, 56.
[24] J. Lagerqvist, M. Zwolak, M. Di Ventra, *Nano Lett.* **2006**, *6*, 779.
[25] B. Luan, H. Peng, S. Polonsky, S. Rossnagel, G. Stolovitzky, G. Martyna, *Phys. Rev. Lett.* **2010**, *104*, 238103.
[26] H. Kwok, K. Briggs, V. Tabard-Cossa, *PLoS One* **2014**, *9*, e92880.
[27] K. Briggs, H. Kwok, V. Tabard-Cossa, *Small* **2014**, *10*, 2077.
[28] E. Beamish, H. Kwok, V. Tabard-Cossa, M. Godin, *Nanotechnology* **2012**, *23*, 405301.
[29] S. W. Kowalczyk, A. Y. Grosberg, Y. Rabin, C. Dekker, *Nanotechnology* **2011**, *22*, 315101.
[30] Q. Chi, G. Wang, J. Jiang, *Phys. A Stat. Mech. its Appl.* **2013**, *392*, 1072.
[31] D. Fologea, M. Gershow, B. Ledden, D. S. McNabb, J. a Golovchenko, J. Li, *Nano Lett.* **2005**, *5*, 1905.
[32] M. Wanunu, J. Sutin, B. McNally, A. Chow, A. Meller, *Biophys. J.* **2008**, *95*, 4716.
[33] J. Larkin, R. Henley, D. C. Bell, T. Cohen-Karni, J. K. Rosenstein, M. Wanunu, *ACS Nano* **2013**, *7*, 10121.
[34] J. Kundu, O. Neumann, B. Janesko, D. Zhang, S. Lal, A. Barhoumi, G. E. Scuseria, N. J. Halas, *J. Phys. Chem. C* **2009**, *113*, 14390.
[35] L. M. Demers, M. Ostblom, H. Zhang, N.-H. Jang, B. Liedberg, C. a Mirkin, *J. Am. Chem. Soc.* **2002**, *124*, 11248.
[36] H. Kimura-Suda, D. Y. Petrovykh, M. J. Tarlov, L. J. Whitman, *J. Am. Chem. Soc.* **2003**, *125*, 9014.
[37] S. W. Kowalczyk, D. B. Wells, A. Aksimentiev, C. Dekker, *Nano Lett.* **2012**, *12*, 1038.